Control of an IMMC-Based Multilevel Converter Using an MPPT–SPWM Strategy for Voltage Balancing of Submodules in Large-Scale Photovoltaic Systems

Tham Nguyen Thi[1,2], Hien Pham Duy[1], Cuong Tran Hung[3] and Phuong Pham Viet[1,*]

[1]*School of Electrical and Electronic Engineering, Hanoi University of Science and Technology, Hanoi, Vietnam*
[2]*Hong Duc University, Thanh Hoa, Vietnam*
[3]*Faculty of Electrical and Engineering, Phenikaa University, Duong Noi, Hanoi, Vietnam*
[*]*Corresponding author E-mail: phuong.phamviet@hust.edu.vn*
DOI: https://doi.org/10.64032/mca.v30i4.454

Abstract

The Isolated Modular Multilevel Converter (IMMC) has emerged as a promising topology for medium-voltage photovoltaic (PV) systems due to its modular architecture and inherent electrical isolation capability. However, in large-scale PV installations, non-uniform solar irradiance across distributed arrays often results in unequal power generation among modules. This condition can lead to voltage imbalance among the converter modules, thereby deteriorating the overall system performance. To overcome this limitation, this paper proposes a unified control strategy for a three-phase IMMC, where each phase consists of two arms, with four modules per arm. The proposed method integrates a DC/DC converter with an enhanced Maximum Power Point Tracking (MPPT) scheme to simultaneously achieve maximum power extraction from each PV source and coordinated power distribution among modules. Through this coordinated control mechanism, voltage balancing among the modules can be inherently achieved without introducing additional balancing control loops. On the inverter side, Sinusoidal Pulse-Width Modulation (SPWM) is employed to synthesize the converter output voltage. Simulation results verify that the proposed control strategy effectively improves voltage balance among the modules, ensures stable converter operation, and enhances dynamic performance under varying irradiance conditions, demonstrating its suitability for large-scale PV applications.

Keywords: *Isolated Modular Multilevel Converter (IMMC); Maximum Power Point Tracking (MPPT); Inherent Voltage Balancing; Coordinated Control Strategy; PV Systems*

Symbols

Symbols	Units	Description
V_i	V	Total voltage of the submodule (SM) in the i-th arm
$v_{i,k}$	V	Voltage of the k-th SM in the i-th arm
v_u, v_l	V	Voltages of the upper and lower arms
v_c	V	Circulating voltage
v_0	V	Output voltage of the IMMC
i_u, i_1	A	Currents of the upper and lower arms
i_0	A	Output phase current
i_c	A	Circulating current within the converter

Abbreviations

IMMC	Isolated Modular Multilevel Converter
MPPT	Maximum Power Point Tracking
PV	Photovoltaic
DC/DC	Direct Current/Direct Current
SPWM	Sinusoidal Pulse-Width Modulation
THD	Total Harmonic Distortion

1. Introduction

Global energy demand continues to increase rapidly due to economic growth and population expansion. However, the heavy reliance on fossil fuels poses significant challenges, including resource depletion, greenhouse gas emissions, and adverse environmental impacts. In addition, recent geopolitical fluctuations have significantly driven up the prices of fuels such as oil and natural gas, directly affecting global energy security [1]. Therefore, the development and integration of renewable energy sources, particularly large-scale solar energy systems, have become an inevitable trend toward achieving sustainable energy systems [2]. In large-scale photovoltaic (PV) systems, power converters play a critical role in energy conversion and in ensuring the quality of the output voltage [3]. Conventional multilevel converter topologies, such as neutral-point-clamped (NPC), flying capacitor (FC), and modular multilevel converters (MMC), have been widely adopted due to their ability to generate high-quality output voltages, reduce harmonic distortion, and minimize switching losses [4]. However, when implemented at the medium-voltage level, these topologies exhibit several major limitations, including limited scalability, complex control requirements, and, notably, the lack of electrical isolation among independent PV sources [5]. To satisfy modern grid-tied PV standards (e.g., IEEE 1547-2018 and IEC TS 62786-1), strict compliance regarding total harmonic distortion (THD), dynamic voltage support, and continuous fault ride-through capabilities is required. Conventional topologies often struggle to meet these stringent requirements without bulky passive filters or complex control schemes. Recently, Isolated Modular Multilevel Converter (IMMC)–based combined with low-frequency transformers have emerged as a promising solution [6], [11–13], offering

Received: 29 June 2026; Revised: 27 July 2026; Accepted: 21 August 2026.

electrical isolation and enhanced operational performance through distributed power characteristics [14]. Nevertheless, a major challenge in IMMC systems lies in maintaining voltage balance across the capacitors of individual submodules, especially under non-uniform operating conditions caused by partial shading or temperature mismatches among PV strings [7], [8]. While foundational studies, such as the work by Verdugo et al., have primarily focused on basic inter-phase and intra-phase energy balancing mechanisms, recent advances in decentralized control strategies and adaptive power allocation schemes have offered significant improvements. Distributed control paradigms enable local submodule controllers to regulate capacitor voltages autonomously using on-site measurements, thereby reducing communication bandwidth requirements, eliminating single-point-of-failure vulnerabilities, and enhancing dynamic response during rapid solar irradiance transients [15], [16].

In addition, the incremental conductance (INC) algorithm has been widely recognized for its high accuracy in maximum power point tracking (MPPT) and its superior ability to reduce oscillations compared to the Perturb and Observe (P&O) method under rapidly changing irradiance conditions [9]. However, existing studies typically focus on optimizing the input power independently, without considering the coordination between MPPT and power distribution within the IMMC structure. Furthermore, Sinusoidal Pulse-Width Modulation (SPWM) is commonly employed to generate high-quality AC output voltages [10]. Nevertheless, when applied independently, it does not fully exploit its potential to support energy balancing among submodules. This lack of coordination may lead to capacitor voltage imbalance, resulting in degraded output voltage quality and reduced system stability [8]. Motivated by the aforementioned challenges, this paper proposes a coordinated control strategy integrating the INC-MPPT algorithm and SPWM for large-scale PV systems employing an IMMC to supply power to the load. The proposed system adopts a multilevel architecture consisting of multiple PV arrays that independently provide DC power to the submodules of a three-phase, multi-arm IMMC, with the output voltage stepped up using a low-frequency transformer. Specifically, each PV source is interfaced with a dedicated DC/DC converter operating under the INC-MPPT algorithm to maximize the extracted power. Meanwhile, SPWM is employed to synthesize the AC output voltage supplied to the load. By regulating the power of individual PV strings, the proposed strategy enables proper energy distribution among IMMC submodules, thereby maintaining capacitor voltage balance without requiring additional complex balancing control loops.

2. Structure of the IMMC in Grid-Connected PV Systems

2.1 Structure of the IMMC

The structure of the IMMC is illustrated in Fig. 1. The system consists of multiple PV sources, each connected to an individual DC/DC converter to regulate the output voltage and enable MPPT for each source. These modules are subsequently integrated into an IMMC to synthesize a three-phase AC output voltage suitable for grid connection [3], [6], [11], [12].

Architecturally, the IMMC is developed based on a modular design principle, in which each submodule consists of an H–bridge inverter integrated with a low-frequency transformer. These submodules are connected in series within each arm, enabling galvanic isolation between the DC and AC sides, while enhancing system scalability and flexibility [6], [11–13].

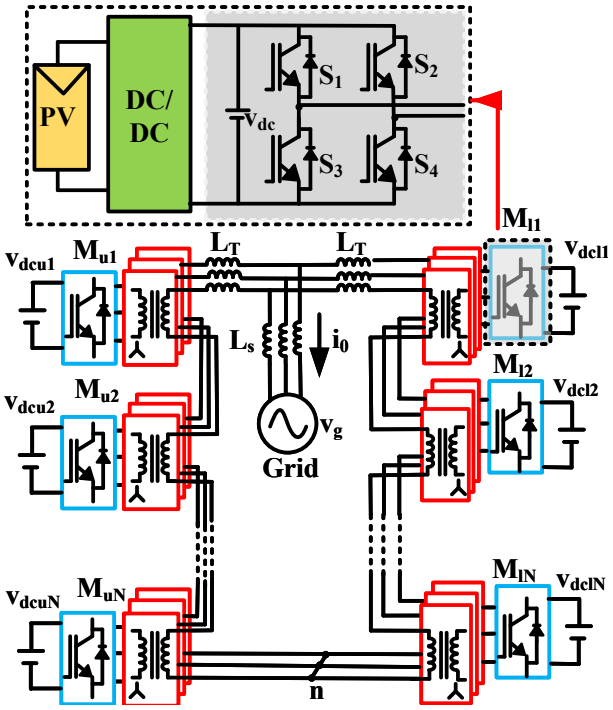


Figure 1: Structure of the IMMC.

The output voltage of the converter is synthesized through the combination of voltages generated by individual submodules. Specifically, the output voltage of each phase is determined by the algebraic sum of the voltages of the submodules within the corresponding arm:

$$v_i = \sum_{k=1}^{N} v_{i,k} \tag{1}$$

where v_i is the total voltage of the i-th arm, $v_{i,k}$ is the voltage of the k-th submodule in the i-th arm, and N is the number of submodules in each arm.

Due to its multilevel structure, the IMMC is capable of improving output voltage quality, reducing harmonic distortion, and minimizing switching losses compared to conventional two-level converters [4], [5].

However, owing to the inherent power mismatch among PV sources, the capacitor voltages of individual submodules tend to become unbalanced, which can significantly degrade system performance and jeopardize stable operation. Therefore, capacitor voltage balancing is regarded as a fundamental requirement in the control of multilevel converters [7], [8], [13], [14].

2.2 Operating Principle of the IMMC

The operating principle of the IMMC is based on the coordination between its multilevel structure and the control system to synthesize high-quality AC voltage from multiple DC sources. In this configuration, the converter current is decomposed into arm currents and internal circulating currents between the upper and lower arms, enabling independent control of power exchange and energy balancing.

The output phase current i_0 is defined as the difference between the currents of the upper and lower arms, which can be expressed as:

$$i_0 = i_u - i_l \tag{2}$$

Meanwhile, the circulating current i_c represents the internal current flowing between the upper and lower arms. It is induced by power imbalance conditions within the converter and can be expressed as follows:

$$i_c = \frac{i_u + i_l}{2} \tag{3}$$

This separation enables the independent control design of the output current and the circulating current, thereby improving system efficiency and operational stability.

The AC voltage of each submodule depends on its DC-link voltage and the corresponding modulation index. The voltage of the k-th submodule in the i-th arm can be expressed as follows:

$$v_{i,k} = \frac{v_{dc,i,k}}{2} \cdot m_{i,k} \tag{4}$$

This circulating current component does not contribute to the output power; however, it is inherently associated with the internal energy exchange among submodules and plays a decisive role in the power distribution mechanism within the converter. If not properly regulated, it may induce low-frequency energy oscillations, which in turn lead to DC-link voltage imbalance across the submodules [7].

Based on (1) and (4), the total synthesized AC voltages generated by the upper and lower arms, denoted as v_u and v_l, are expressed as:

$$\begin{aligned} v_u &= \sum_{k=1}^{N} \frac{v_{dc,u,k}}{2} m_{u,k} \\ v_l &= \sum_{k=1}^{N} \frac{v_{dc,l,k}}{2} m_{l,k} \end{aligned} \tag{5}$$

where $v_{dc,u,k}$ and $v_{dc,l,k}$ are the DC-link voltages and $m_{u,k}$, $m_{l,k}$ represent the modulation indices of the k-th submodule in the upper and lower arms, respectively.

To regulate the output and circulating currents, the synthesized arm voltages (v_s, v_c) and the corresponding modulation indices (m_u, m_l) are formulated as:

$$\begin{aligned} v_s &= \frac{-v_u + v_l}{2} \\ v_c &= -\frac{v_u + v_l}{2} \end{aligned} \tag{6}$$

Based on the above formulation, the modulation indices of the upper and lower arms are derived to achieve effective submodule control.

$$\begin{aligned} m_u &= \frac{2}{V_{\Sigma_{dc}}}(v_c - v_s) \\ m_l &= \frac{2}{V_{\Sigma_{dc}}}(v_c + v_s) \end{aligned} \tag{7}$$

where v_c represents the control voltage component associated with the circulating current. By adjusting these modulation coefficients, the converter can simultaneously regulate the output current and the circulating current, thereby ensuring an appropriate power distribution among the submodules.

Through this coordinated control mechanism, the submodules within the IMMC are able to operate in a fully coordinated manner to synthesize high-quality multilevel AC voltages, while effectively suppressing internal energy oscillations and ensuring stable capacitor voltage balancing. This aspect is particularly critical in large-scale PV systems, where inherent power mismatches among distributed sources may significantly deteriorate overall system performance and compromise operational stability.

For the purpose of controller design and system analysis, the mathematical model of the IMMC is developed based on the power circuit schematic shown in Fig. 2.

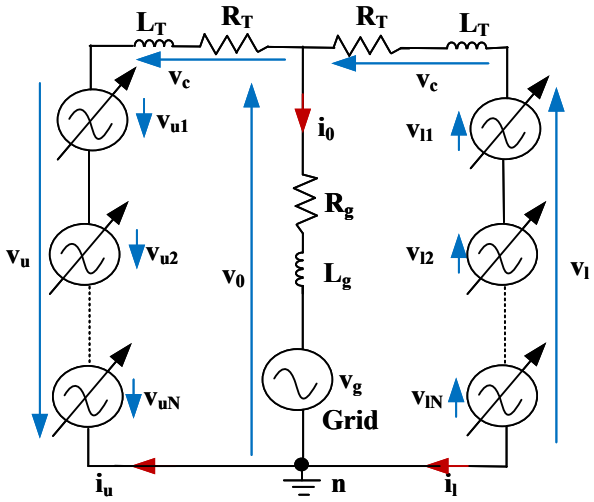


Figure 2: Modeling of the IMMC Structure.

The converter is modeled as two power arms corresponding to the upper and lower arms, which are interconnected through equivalent inductive and resistive elements.

By applying Kirchhoff's voltage law to the circuit loops, the voltage equations of the system can be formulated as follows:

$$\frac{L_T}{2}\frac{di_0}{dt} + \frac{R_T}{2} i_0 = -\frac{v_u + v_l}{2} - v_0 \tag{8}$$

where v_u and v_l denote the voltages of the upper and lower arms, respectively; i_0 is the output current, and v_0 is the converter output voltage. Similarly, the dynamic equation of the circulating current can be expressed as follows:

$$L_T \frac{di_c}{dt} + R_T i_c = v_c \tag{9}$$

where v_c represents the control voltage component associated with the internal circulating current. Equations (8) and (9) indicate that the output current and the circulating current can be independently controlled through their corresponding voltage components, which constitutes a fundamental basis for the design of control strategies for the IMMC [7], [8]. In addition, the power of each arm in the converter can be determined as the product of its corresponding voltage and current.

The power of each arm in the converter is determined as the product of its corresponding voltage and current. Specifically, the powers of the upper and lower arms can be expressed as

follows:

$$P_u = v_u i_u$$
$$P_l = v_l i_l \tag{10}$$

By decomposing the current components into i_0 and i_c, the total power of the system can be expressed as follows:

$$P = P_u + P_l = -v_0 i_0 - 2v_c i_c \tag{11}$$

Equation (11) indicates that the total system power consists of two main components: the power exchanged with the grid through the output current i_0, and the internal power associated with the circulating current i_c. This internal power component plays a crucial role in energy distribution and in maintaining capacitor voltage balance among the submodules.

Under ideal conditions, where losses in the equivalent resistance R_T and inductance L_T are neglected, the voltage drops across these elements can be assumed negligible. Consequently, recalling the current relationships in (2) and (3), the maximum power that the system can deliver is expressed as:

$$P_{\max} = 2V_0 I_{0(\max)} \tag{12}$$

where V_0 and $I_{0(\max)}$ denote the output voltage magnitude and the maximum allowable output current, respectively.

These results demonstrate that the IMMC converter is capable of handling high power transfer with multilevel output voltage, while reducing power losses and improving the overall system efficiency compared to conventional converter topologies.

3. Control Strategy for the IMMC Converter

3.1 MPPT-INC Algorithm

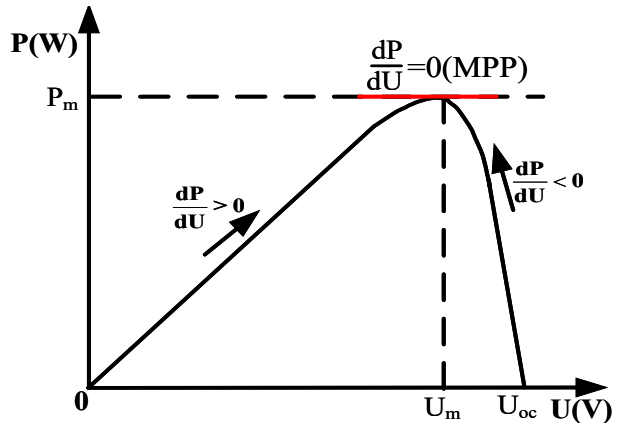


Figure 3: PV characteristic curve and the MPP.

In PV systems, the MPPT algorithm plays a crucial role in maximizing the harvested power under varying irradiance and temperature conditions [9]. For IMMC-based multi-level converter structures, integrating MPPT at the control level enables each PV string to operate close to its maximum power point (MMP), thereby enhancing the overall system efficiency, particularly under non-uniform irradiance conditions [11], [12].

Among various MPPT methods, the INC algorithm is widely adopted due to its ability to accurately locate the MPP and its strong adaptability to rapidly changing environmental conditions [9]. The principle of the INC method is based on the condition at the maximum power point:

$$\frac{dP}{dV} = 0 \implies \frac{dI}{dV} = -\frac{I}{V} \tag{13}$$

Based on this relationship, the operating point of the system is determined using the INC algorithm, as illustrated in Fig. 3.

From this, the operating state of the system can be determined as follows [12]:

If $\frac{\Delta I}{\Delta V} = -\frac{I}{V}$, the system operates at the MPP.

If $\frac{\Delta I}{\Delta V} > -\frac{I}{V}$, the system operates on the left-hand side of the MPP, where the incremental conductance is positive.

If $\frac{\Delta I}{\Delta V} < -\frac{I}{V}$, the system operates on the right-hand side of the MPP, where the incremental conductance is negative.

Based on this criterion, the duty cycle of the DC/DC converter is regulated to steer the operating point toward the MPP.

However, the main drawback of the conventional INC method lies in the use of a fixed step size, which results in a trade-off between convergence speed and steady-state power oscillation [15]. A large perturbation step improves the convergence speed but induces significant oscillations around the MPP, whereas a small step enhances steady-state stability but slows down the tracking response [18], [19].

3.2 Improved MPPT-INC Algorithm

To overcome the aforementioned limitation, this paper proposes an improved MPPT-INC algorithm based on an adaptive step-size mechanism driven by the slope of the power-voltage (P-V) characteristic. The core idea is to adjust the step size according to the value of $\left|\frac{dP}{dV}\right|$, thereby reflecting the degree of deviation from the MPP [17–19].

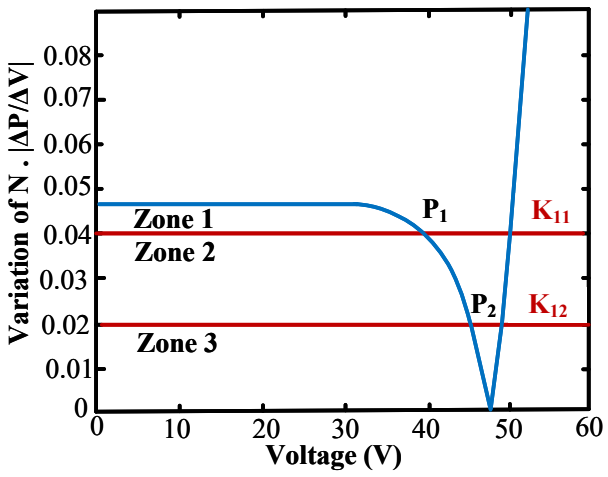


Figure 4: Change in the slope of the P–V characteristic.

The update law can be expressed as follows:

$$D(k) = D(k-1) \pm N\left|\frac{\Delta P}{\Delta V}\right| \tag{14}$$

where N is a positive proportional gain that determines the sensitivity of the adjustment step. Accordingly, the operating region around the MPP is divided into three main regions, as illustrated in Fig. 4.

Region 1 (far from the MPP): The slope is large, corresponding to a significant deviation from the MPP. A large

adjustment step is employed to reduce the convergence time [17].

Region 2 (near the MPP): The slope decreases, and the adjustment step is reduced to suppress oscillations and improve transient performance [18].

Region 3 (at the MPP): When $\left|\frac{\Delta P}{\Delta V}\right| \to 0$, operating at the maximum power point (MPP), the adjustment step approaches a very small value, thereby reducing power oscillations and improving steady-state accuracy [19].

The incorporation of a variable step-size mechanism allows the improved INC algorithm to effectively mitigate the inherent limitations of the conventional approach, thereby significantly enhancing the overall MPPT performance.

Fig. 5 illustrates the complete operational flowchart of the proposed INC algorithm.

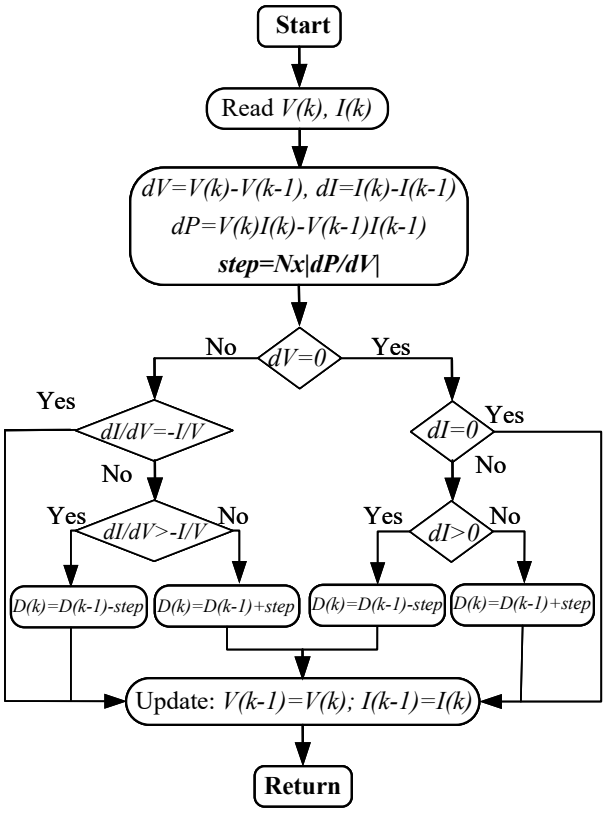


Figure 5: Flowchart of the proposed improved MPPT–INC algorithm.

In comparison with the conventional INC approach, the proposed improved MPPT–INC algorithm achieves faster transient response, effectively suppresses power and current oscillations, and exhibits superior adaptability to rapid variations in solar irradiance and ambient temperature conditions [17–19].

Furthermore, the incorporation of a slope-adaptive mechanism improves the MPP tracking capability in multilevel and distributed photovoltaic systems, such as IMMC structures, where mismatches among PV branches may significantly degrade the overall system performance [11],[12].

3.3 PWM Modulation for the IMMC

To control the semiconductor switches of the IMMC converter, the SPWM technique is adopted to enhance output voltage quality and reduce THD. Fundamentally, this technique operates by comparing a sinusoidal reference signal v_{ref} with a high-frequency triangular carrier signal v_{car}. When $v_{\text{ref}} > v_{\text{car}}$, the corresponding switch is activated; otherwise, it is deactivated. This high-frequency switching action produces a sequence of voltage pulses whose average value follows a sinusoidal trajectory, thereby generating a multilevel output voltage waveform that closely approximates an ideal sinusoid [8], [10].

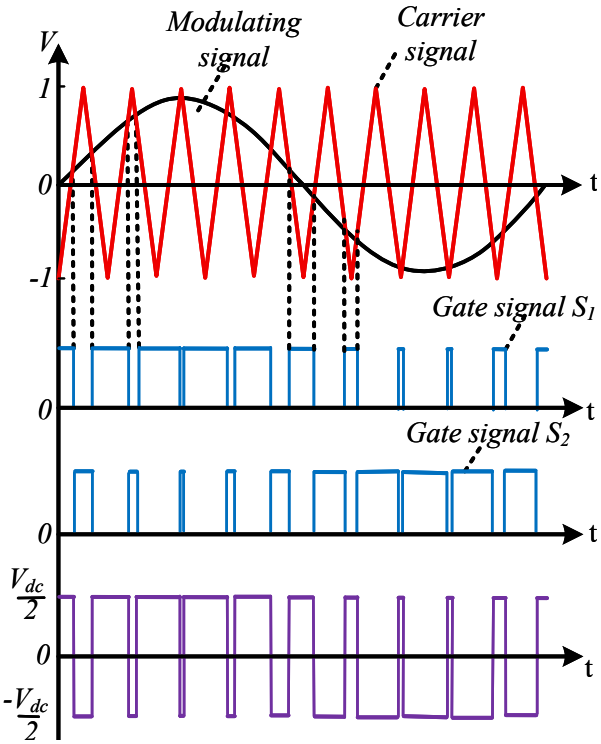


Figure 6: Schematic diagram of the SPWM technique.

The phase reference voltage signal of the converter is mathematically defined as follows:

$$v_{\text{ref}} = v_m \sin(\omega t + \phi) \tag{15}$$

where v_{m} denotes the reference voltage amplitude, ω represents the angular frequency, and ϕ denotes the initial phase angle.

For an IMMC topology with N submodules per arm, in order to ensure that the synthesized output voltage accurately tracks the reference signal, the control signal for each submodule is normalized as follows:

$$m_i(t) = \frac{v_{\text{ref}}}{N \cdot V_{\text{dc}}}; \quad i = 1, 2, 3, \ldots, N \tag{16}$$

where v_{dc} represents the average DC-link voltage per submodule.

In order to enhance the output voltage quality without raising the switching frequency of each individual semiconductor device, a set of triangular carrier signals with equal amplitude and switching frequency f_{sw} are evenly phase-shifted by an angle: $\Delta\varphi = \frac{2\pi}{N}$.

Hence, the triangular carrier signal of the i-th submodule is defined as follows:

$$c_i(t) = c\left(t - \frac{(i-1)T_{\text{sw}}}{N}\right) \tag{17}$$

where $T_{\text{sw}} = \frac{1}{f_{\text{sw}}}$ is the switching period of the semiconductor device.

The gating signal for each submodule is obtained by comparing the modulating signal with the carrier signal:

$$v_i(t) = \begin{cases} 1 & \text{if } m_i(t) \geq c_i(t) \\ 0 & \text{if } m_i(t) < c_i(t) \end{cases} \tag{18}$$

Equation (18) defines the relationship between the modulating signal $m_i(t)$ and carrier signal $c_i(t)$, governing the semiconductor switching states. Here, the amplitude of $m_i(t)$ shapes the output voltage, while the frequency of $c_i(t)$ determines the system switching frequency. Utilizing phase-shifted carriers evenly distributes switching stress across submodules and elevates the effective output frequency by a factor of N relative to individual devices. Consequently, the THD is substantially reduced without increasing switching frequencies or losses [8], [10].

Furthermore, normalizing submodule-level modulation signals enables flexible voltage and power distribution, which is critical for grid-connected PV systems under non-uniform irradiance or partial shading. Ultimately, the proposed SPWM strategy ensures output power quality compliance while promoting energy balancing and DC-link voltage stabilization, thereby enhancing the overall efficiency and reliability of the IMMC topology.

4. Simulation Results and Discussion

Based on the theoretical analysis and the developed mathematical model, the IMMC is implemented in a simulation environment to evaluate its performance in grid-connected PV systems and to validate the effectiveness of the proposed control strategy. In this study, the MPPT algorithm using the INC method is integrated with SPWM modulation to ensure maximum power extraction from the PV sources while maintaining voltage balance across the DC-link capacitors of the submodules.

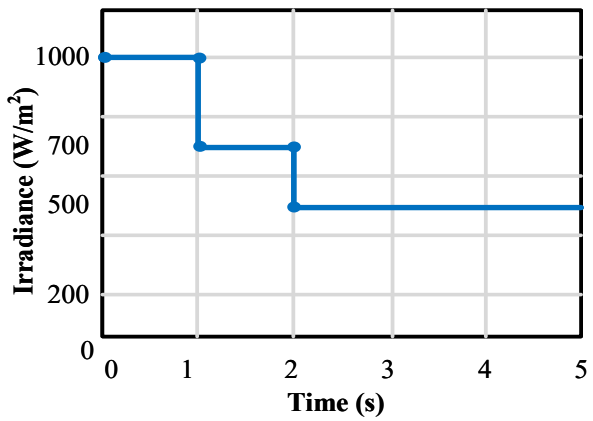


Figure 7: Solar Irradiance Profile.

To accurately assess the MPPT capability under dynamic irradiance conditions, the solar irradiance profile is varied in a stepwise manner from 1000 to 700 and 500 W/m^2, as depicted in Fig. 7. A three-phase IMMC topology comprising four submodules per arm is adopted as the investigated system. The corresponding system parameters are summarized in Table 1.

Table 1: Simulation Parameters

Parameter	Symbol	Value
PV Array		
Array configuration	SunPower SPR-305E-WHT-D	6×3
DC/DC Converter		
Inductance	L	0.5 mH
Capacitance	C	4.7 μF
Resistance	R	0.01 Ω
DC/AC Inverter		
Inductance	L_{T}	0.1 mH
Number of modules	N	4
Switching frequency	f_{c}	2500 Hz
Transformer Parameters		
Transformer power rating	S_{T}	2.5 MW
Transformer ratio	r_{T}	1:2
Winding inductance	L_{r}	7.6 mH
Operating frequency	f_{r}	50 Hz

4.1 Output Characteristics Analysis of the PV Array

Fig. 8 shows the dynamic response of I_{PV}, V_{PV}, and P_{PV}. At nominal irradiance (1000 W/m^2, 0–1 s), the system reaches steady-state maximum power at ≈ 5.5 kW ($I_{\mathrm{PV}} \approx 17$ A, $V_{\mathrm{PV}} \approx 330$ V). When irradiance drops to 700 W/m^2 (at 1 s) and 500 W/m^2 (at 2 s), P_{PV} decreases to ≈ 3.8 kW and ≈ 2.8 kW, respectively. Meanwhile, V_{PV} remains tightly regulated near the MPP with minimal transient deviation, confirming the rapid tracking and robust stability of the proposed MPPT under environmental step-changes.

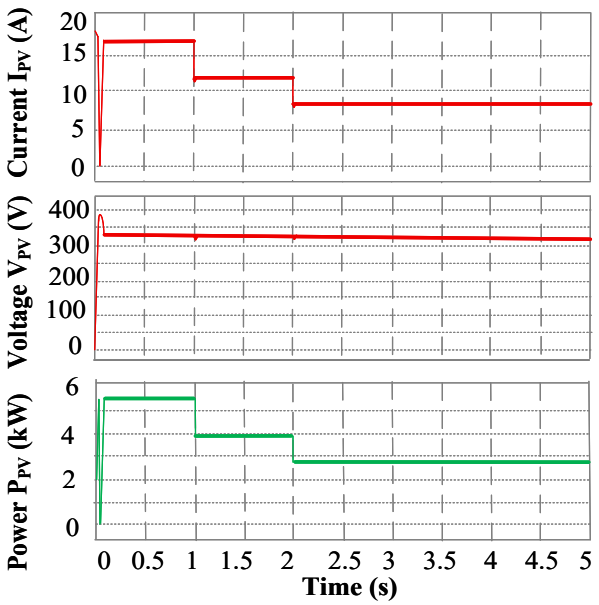


Figure 8: Output characteristics of the PV array.

4.2 DC-Link Voltage Analysis

Fig. 9 shows the DC-link voltage dynamic response at the DC/DC converter output. During startup (0–1 s), as energy accumulates in the DC-link capacitors, V_{DC} increases smoothly from 0 V to a steady-state value of ≈ 2.1 kV. At irradiance drops (1 s and 2 s), reduced PV input power causes a slight transient drop in V_{DC}. However, V_{DC} is quickly regulated back to ≈ 1.95 kV. These results demonstrate that the DC/DC converter effectively boosts voltage while acting as an energy buffer, mitigating PV power fluctuations on the downstream

system.

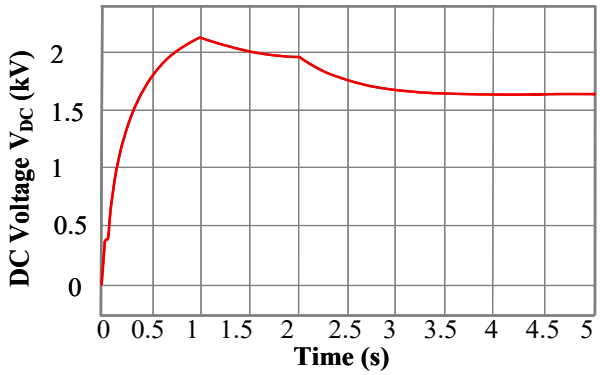


Figure 9: DC-link voltage V_{dc} of the DC/DC converter.

4.3 Analysis of the Arm Voltage and Current of the IMMC

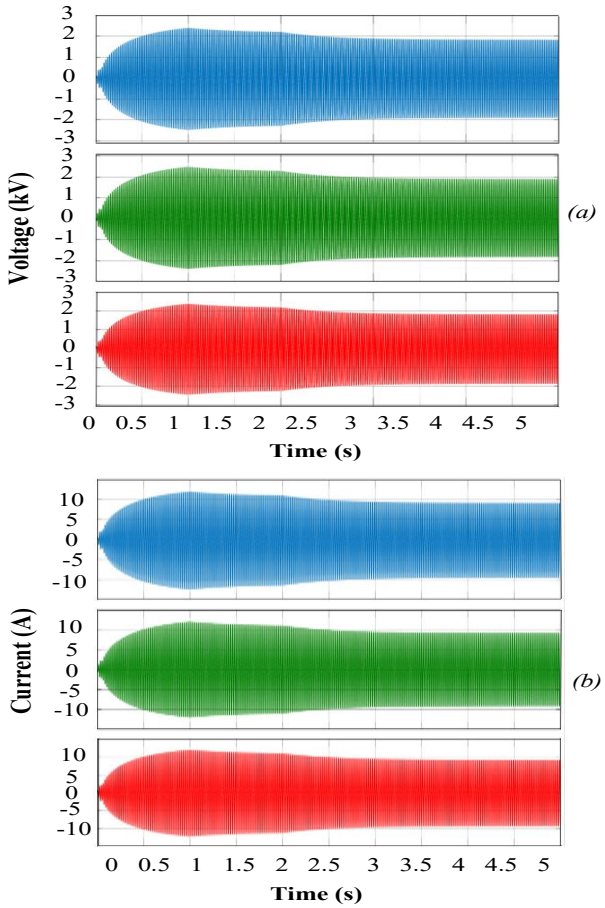


Figure 10: Arm voltage and current of the IMMC.
(a) Upper-arm, lower-arm, and total phase voltage (for one phase);
(b) Upper-arm, lower-arm, and total phase current (for one phase).

Fig. 10 presents the voltage and current waveforms of the IMMC, including the upper-arm, lower-arm, and phase quantities. As shown in Fig. 10a, the arm voltages exhibit a symmetric multilevel staircase waveform centered around zero, consistent with the operating principle of multilevel converters. The voltage is synthesized from the submodule capacitor voltages and remains consistent with the regulated DC-link voltage V_{DC}, demonstrating effective modulation and accurate voltage synthesis. Furthermore, no significant voltage imbalance is observed among the submodules, confirming that the proposed control strategy achieves effective self-voltage balancing without requiring additional balancing circuits.

For the current waveforms in Fig. 10b, the upper and lower-arm currents are nearly sinusoidal and exhibit a high degree of symmetry, resulting in a stable sinusoidal phase current. No abnormal oscillations or current interruptions are observed, indicating stable power transfer between the converter arms. Furthermore, the internal circulating currents are effectively suppressed, thereby reducing conduction losses, mitigating stress on the semiconductor devices, and contributing to stable capacitor voltage regulation. These results verify the proper operation of the IMMC and its capability to maintain balanced energy distribution between the upper and lower arms.

4.4 Analysis of the Three-Phase Grid-Connected Output Voltage and Current

Fig. 11 shows the three-phase output currents of the IMMC. The phase currents are sinusoidal and shifted by 120°, rendering a balanced system. As shown in Fig. 11a, the output current amplitude (lower plot) varies smoothly with solar irradiance, tracking the PV power variations throughout the simulation. No overshoot or current spikes occur. Meanwhile, the grid voltage peak (upper plot) remains stable at ≈ 1.9 kV, demonstrating effective voltage regulation despite input power fluctuations.

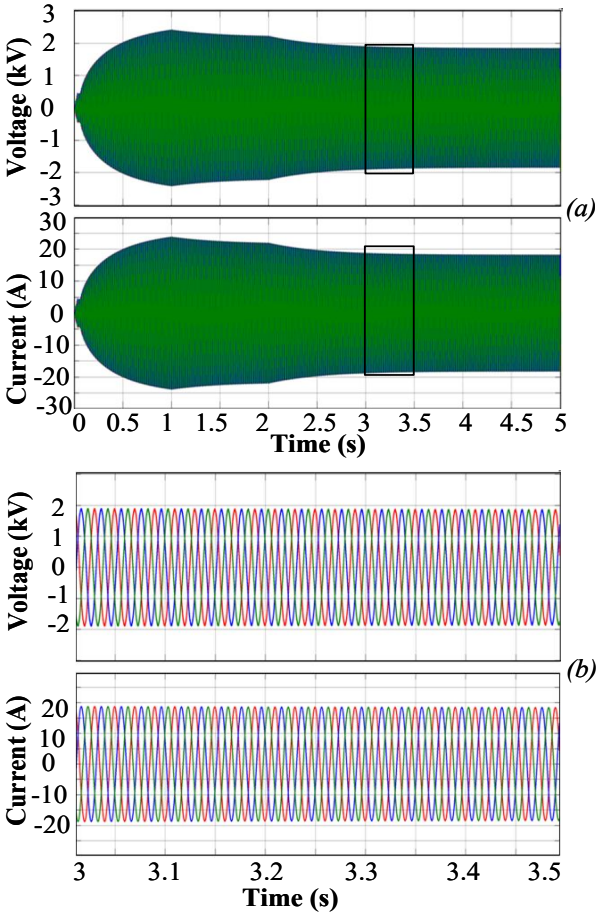


Figure 11: Three-phase output voltage and current of the IMMC.
(a) Three-phase voltage and current under irradiance variation conditions;
(b) Detailed view of three-phase voltage and current under irradiance variation conditions from 3 s to 3.5 s.

A closer observation under conditions from 3 to 3.5 s in Fig. 11b reveals that the output voltage and current waveforms exhibit high quality. The phase waveforms (red, green, and blue) are smooth sinusoidal signals, maintaining strict symmetry and a precise 120° phase shift between each other, thereby confirming that unwanted reactive power components are effectively eliminated.

4.5 Output Harmonic Analysis

To evaluate power quality prior to grid connection, FFT harmonic spectra of the output waveforms are shown in Fig. 12. At the 50 Hz fundamental frequency, the total harmonic distortion is 1.15% for the output voltage in Fig. 12a and 0.21% for the grid current in Fig. 12b—both well below the IEEE 519 standard threshold of 5%. These results confirm that the proposed IMMC with SPWM effectively attenuates high-order switching harmonics.

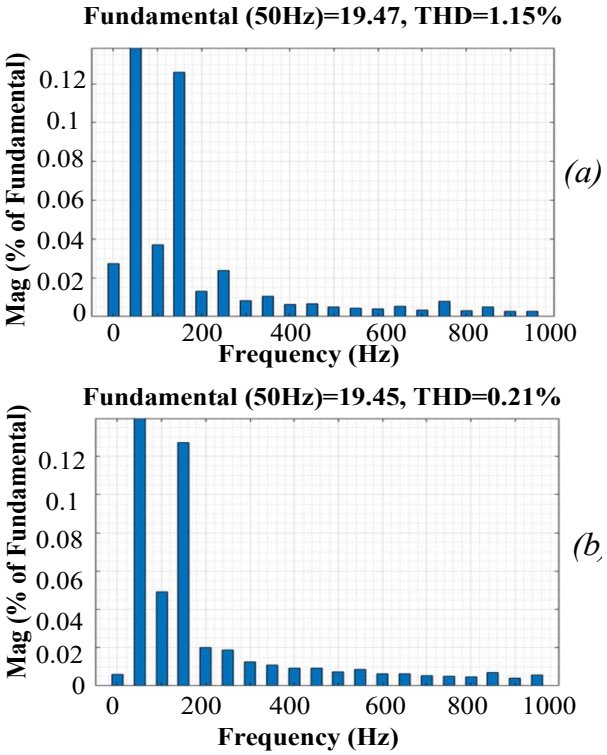


Figure 12: FFT analysis results under steady-state conditions.
(a) FFT analysis result of the output voltage;
(b) FFT analysis result of the output current.

4.6 Analysis of Robustness and Sensitivity

To evaluate the efficacy of the IMMC control scheme employing the MPPT–SPWM strategy under non-ideal operating conditions and hardware parameter deviations, a series of efficacy tests and sensitivity analyses were conducted.

4.6.1 Operation Under Inter-Module Irradiance Mismatch

Under severe irradiance mismatch—where the irradiance of submodule SM1 in Phase A steps down from 1000 to 300 W/m^2, while the remaining submodules step down from 1000 to 700 and 500 W/m^2 (at $t = 1$ s and $t = 2$ s, respectively)—the control strategy effectively maintains inter-phase power balance, achieving a low grid current THD of 0.79% Fig. 13.

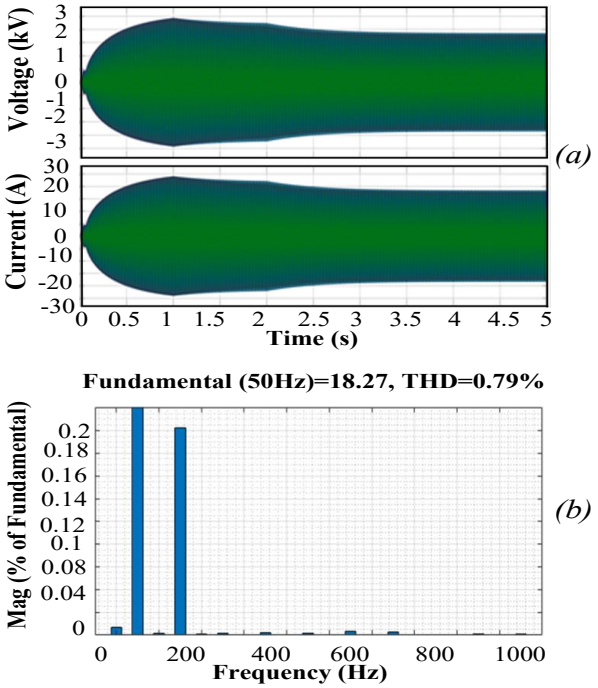


Figure 13: Irradiance Mismatch.
(a) Three-phase output voltage and current of the IMMC;
(b) FFT analysis result of the output current.

4.6.2 Comparison with Conventional INC

To highlight the superiority of the proposed approach over the conventional INC method, system performance was benchmarked under identical conditions. As shown in Fig. 14a, the proposed control strategy suppresses the power oscillations and tracking chatter inherent to conventional INC, yielding smooth three-phase output voltages and currents. Additionally, the FFT spectrum in Fig. 14b confirms that conventional INC produces a higher grid current THD of 0.82% compared to the proposed scheme.

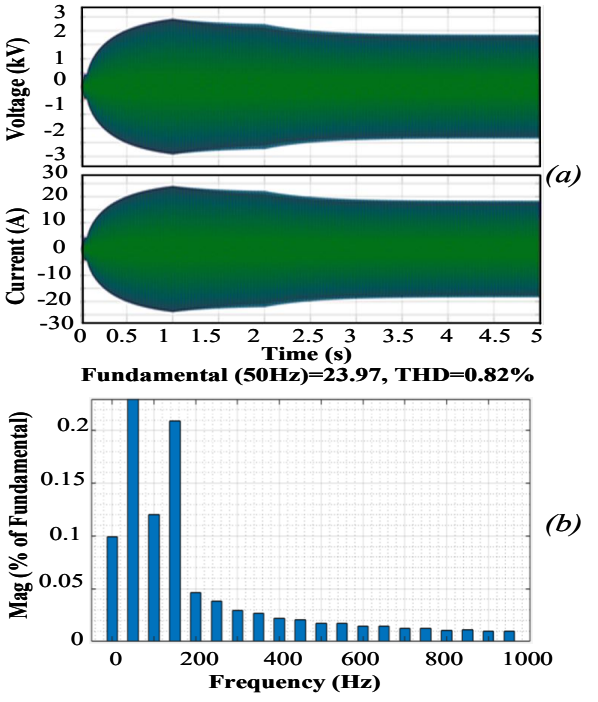


Figure 14: Comparison with Conventional INC.
(a) Three-phase output voltage and current of the IMMC;
(b) FFT analysis result of the output current.

4.6.3 Robustness Under Real-World Operating Conditions

The efficacy of the proposed control strategy was further evaluated considering a 20% capacitance reduction in one of the Phase A submodules due to component aging. As presented in Fig. 15, the algorithm maintains balanced output power sharing while achieving a low grid current THD of 0.81%. These findings confirm the practical viability of the proposed controller under non-ideal operating conditions.

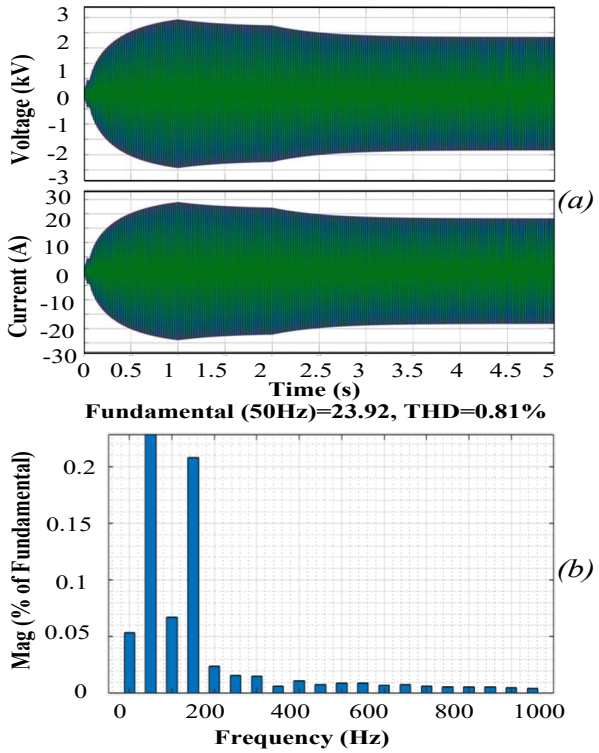


Figure 15: Hardware non-idealities–Capacitor aging.
(a) Three-phase output voltage and current of the IMMC;
(b) FFT analysis result of the output current.

Table 2: Performance Evaluation of the Proposed Method Under Different Operating Scenarios

Scenario	Efficiency (%)	Grid THD (%)
Proposed Method (Baseline)	**95.2**	**0.21**
Irradiance Mismatch	93.0	0.79
Capacitor Aging	88.0	0.81
Conventional INC	86.66	0.82

Based on the simulation results summarized in Table 2, the proposed method consistently outperforms the conventional INC algorithm in terms of both conversion efficiency and current THD. Furthermore, the control strategy maintains high operational efficacy even under hardware non-idealities, confirming its superior performance and robustness.

5. Conclusion

This paper presented the modeling and simulation of a three-phase IMMC for large-scale PV systems using an adaptive MPPT–INC algorithm and an SPWM strategy. The simulation results demonstrated stable operation under varying irradiance conditions while maintaining balanced power distribution among the converter modules and generating a near-sinusoidal output voltage. The proposed adaptive MPPT–INC algorithm achieved fast and accurate maximum power tracking, thereby maximizing energy extraction from the PV arrays while ensuring low THD for both output current and voltage to satisfy grid-connection technical requirements.

Furthermore, the efficacy of the proposed control strategy was thoroughly validated under practical non-ideal conditions, including severe irradiance mismatches and submodule capacitance degradation due to component aging. Even under these parameter mismatch scenarios, the controller effectively maintained inter-module power balance and strict grid compliance. Comparative evaluation confirms that the proposed scheme consistently outperforms the conventional fixed-step INC algorithm across all operating scenarios in terms of both power conversion efficiency and harmonic suppression. These findings establish the proposed IMMC with adaptive MPPT–INC as a reliable, highly efficient, and practically viable solution for large-scale PV applications.

References

[1] International Energy Agency (IEA), *World Energy Outlook 2022*. Paris, France: IEA, 2022. [Online]. Available: https://www.iea.org/reports/world-energy-outlook-2022

[2] O. A. Al-Shahri, F. B. Ismail, M. A. Hannan, M. S. H. Lipu, and A. Q. Al-Shetwi, "Solar photovoltaic energy optimization methods, challenges and issues: A comprehensive review", *Journal of Cleaner Production*, vol. 284, p. 125 465, 2021. DOI: 10.1016/j.jclepro.2020.125465

[3] A. Q. Al-Shetwi and M. Z. Sujod, "Grid-connected photovoltaic power plants: A review of the recent integration requirements in modern grid codes", *International Journal of Energy Research*, vol. 42, no. 5, pp. 1849–1865, 2018. DOI: 10.1002/er.3383

[4] A. Bughneda, M. Salem, A. Richelli, D. Ishak, and S. Alatai, "Review of multilevel inverters for pv energy system applications", *Energies*, vol. 14, no. 6, p. 1585, 2021. DOI: 10.3390/en14061585

[5] S. Kouro et al., "Recent advances and industrial applications of multilevel converters", *IEEE Transactions on Industrial Electronics*, vol. 57, no. 8, pp. 2553–2580, 2010. DOI: 10.1109/TIE.2010.2049719

[6] Q. Shuan, J. L. Bhattacharya, and S. S. Mani, "Isolated modular multilevel converter (immc) for grand-scale solar photovoltaic (pv) integration", *IEEE Transactions on Power Electronics*, vol. 35, no. 8, pp. 8012–8025, 2020. DOI: 10.1109/TPEL.2020.2965412

[7] S. Debnath, J. Jiang, and M. Chinthavali, "Features and performance review of modular multilevel converter topologies, modeling, control schemes, and voltage balancing methods", *IEEE Transactions on Power Electronics*, vol. 30, no. 11, pp. 6054–6068, 2015. DOI: 10.1109/TPEL.2014.2375550

[8] M. A. Perez, S. Bernet, J. Rodriguez, S. Kouro, and R. Lizana, "Circuit topologies, modeling, control schemes, and applications of modular multilevel converters", *IEEE Transactions on Power Electronics*, vol. 30, no. 1, pp. 4–17, 2015. DOI: 10.1109/TPEL.2014.2310127

[9] K. Jain, M. M. Gupta, and A. K. Bohre, "Implementation and comparative analysis of p&o and inc mppt method for pv system", in *Proceedings of the 8th IEEE India International Conference on Power Electronics (IICPE)*, 2018, pp. 1–6. DOI: 10.1109/IICPE.2018.8709519

[10] K. Bano, G. Abbas, M. Hatatah, E. Touti, A. Emara, and P. Mercorelli, "Phase shift apod and pod control technique in multi-level inverters to mitigate total harmonic distortion", *Mathematics*, vol. 12, no. 5, p. 656, 2024. DOI: 10.3390/math12050656

[11] C. Verdugo, J. I. Candela, and P. Rodriguez, "Energy balancing with wide range of operation in the isolated multi-modular converter", *IEEE Access*, vol. 8, pp. 84 479–84 489, 2020. DOI: 10.1109/ACCESS.2020.2992383

[12] C. Verdugo, J. I. Candela, and P. Rodriguez, "Three-phase isolated multi-modular converter in renewable energy distribution systems", *IEEE Journal of Emerging and Selected Topics in Power Electronics*, vol. 8, no. 1, pp. 854–865, 2020.

[13] C. Verdugo, J. I. Candela, F. Blaabjerg, and P. Rodriguez, "Model and control of the isolated multi-modular converter", in *Proc. ECON 2017 – 43rd Annual Conference of the IEEE Industrial Electronics Society*, 2017.

[14] C. Verdugo, J. I. Candela, and P. Rodriguez, "Quadrature voltage compensation in the isolated multi-modular converter", *Energies*, vol. 14, no. 3, p. 529, 2021. DOI: 10.3390/en14030529

[15] M. Vivert et al., "Decentralized control for balancing the cell voltages of a high conversion ratio flying capacitor multilevel converter", *IEEE Journal of Emerging and Selected Topics in Industrial Electronics*, vol. 3, no. 3, pp. 635–646, 2022. DOI: 10.1109/JESTIE.2021.3115958

[16] Q. D. Phan et al., "Decentralized capacitor voltage control of flying capacitor multilevel inverter", *International Symposium on Electrical and Electronics Engineering (ISEE)*, pp. 238–243, 2021. DOI: 10.1109/ISEE51682.2021.9418671

[17] R. B. Bollipo, S. Mikkili, and P. K. Bonthagorla, "Hybrid, optimal, intelligent and classical pv mppt techniques: A review", *CSEE Journal of Power and Energy Systems*, vol. 7, no. 1, pp. 9–33, 2021. DOI: 10.17775/CSEEJPES.2019.02720

[18] R. B. Bollipo, S. Mikkili, and P. K. Bonthagorla, "Critical review on pv mppt techniques: Classical, intelligent and optimisation", *IET Renewable Power Generation*, vol. 14, no. 9, pp. 1433–1452, 2020. DOI: 10.1049/iet-rpg.2019.1163

[19] Wellawatta and S.-J. Choi, "An improved incremental conductance mppt method for the photovoltaic generation", in *Proceedings of the Korean Institute of Power Electronics (KIPE) Annual Conference*, 2016, pp. 185–186. [Online]. Available: http://www.dbpia.co.kr/Article/NODE0671642